ЖЭТФ, 2009, том 136, вып. 2 (8), стр. 362–368

MEASUREMENTS OF WORK FUNCTION OF PRISTINE AND CuI DOPED CARBON NANOTUBES

A. A. Zhukov [a*], ***V. K. Gartman*** [a], ***D. N. Borisenko*** [a], ***M. V. Chernysheva*** [b], ***A. A. Eliseev*** [b]

[a] *Institute of Solid State Physics, Russian Academy of Sciences*
142432, Chernogolovka, Moscow Region, Russia

[b] *M. V. Lomonosov Moscow State University*
119991, Moscow, Russia

Received March 2, 2009

We report the results on measurements of the work function of carbon nanotubes and carbon-nanotube-based materials including pristine multi-walled and single-walled carbon nanotubes as well as single-walled carbon nanotubes intercalated by CuI with the Kelvin probe technique. We found the work function value 4.97–4.98 eV for pristine carbon nanotubes, while carbon nanotubes infilled with CuI demonstrate the work function value decreased by more than 0.1 eV (4.86–4.96 eV).

PACS: 72.80.Rj, 73.21.Hb, 73.23.-b

1. INTRODUCTION

The discovery of carbon nanotubes [1] triggered increased interest in carbon-nanotube-based materials, motivated by their unique electronic and mechanical properties and suggesting their possible application in electronic devices [2]. It is generally accepted that all the properties of carbon nanotubes strongly depend on the tube diameter and chirality [3] and can be successfully influenced by chemical modification of the tubular external surface (e.g., decoration or coating) [4] or their internal channels (e.g., intercalation) [5, 6]. For example, superconductivity was found in C_{60} fullerene doped with Rb or Cs [7]. Doping of carbon nanotubes alternates not only the value of their conductivity [8] but also their work function Φ [9]. An essential change of positions of the conductance and valence bands was also observed previously [5]. Decreasing the value of the work function [9] with doping opens an additional possibility for using carbon nanotubes as electron emitters. In this paper, we present a set of measurements of the work function for pristine multi-walled and single-walled carbon nanotubes as well as for single-walled carbon nanotubes intercalated by CuI with Kelvin probe microscopy. This technique was confirmed to be an effective method to investigate electronic properties of the carbon nanotube and carbon-nanotube-based field-effect transistors [10–13]. We also compare noncontact Kelvin probe measurements with local differential capacitance measurements (LCM).

This paper is organized as follows. In Sec. 2, we describe sample preparation, tube growth, and doping procedures and give a detailed description of scanning methods we used; in Sec. 3, we present experimental results and discussion; Sec. 4 is a conclusion.

2. EXPERIMENTAL DETAILS

In our experiment, we used a standard silicon/silicon oxide wafer. The thickness of SiO_2 was 1000 nm, and p-type doped silicone substrate served as a back gate. On the surface of SiO_2, a Pd mesh was formed by optical lithography.

Multi-walled carbon nanotubes (MWCNTs) were grown by electric arc-discharge method described in [14]. Single-walled carbon nanotubes (SWCNTs) were formed by catalytic arc-discharge method using graphite rods 0.8 cm in diameter with Y/Ni powder catalyst at the 73.3 kPa helium pressure and the current 100–110 A [15]. The SWCNTs were purified by a multistage procedure consisting in controllable oxygenation in air and rinsing by HCl for catalyst removal [16]. To form CuI intercalated SWCNTs, the purified

*E-mail: azhukov@issp.ac.ru

nanotubes with the SWCNT content of 86 wt.% and the catalyst content of less than 0.1 wt.% were preopened by temperature treatment at 500 °C in dry air for 0.5 h. The oxidized SWCNTs (0.025 g) were grinded with 0.4 g of CuI (Aldrich, 99 wt.%) in agate mortar, vacuumized at 10^{-5} mbar for 3 h, and sealed into a quartz ampoule. The sample was treated at 705 °C (100 °C above the melting point of CuI) for 6 h and slowly cooled (0.02 °C/min) to room temperature to induce better crystallization.

The SWCNTs intercalated by CuI have been investigated using Raman spectroscopy [17] and high-resolution transmission electron microscopy [18]. It was shown that RB (radial breathing) and G modes of the Raman spectrum of this material demonstrates strengthening of C–C bonds due to charge transfer from nanotube walls onto the intercalated CuI nanocrystal. This behavior is typical of acceptor-type impurities intercalated into single-walled carbon nanotubes [19, 20]. In [18], a comprehensive analysis of the structure of one-dimensional CuI nanocrystals in SWCNT channels was reported. It was concluded that CuI nanocrystal grew inside a SWCNT with either $\langle 001 \rangle$ or $\langle 1\bar{1}0 \rangle$ crystallographic axes aligned along the SWCNT depending on the channel diameter.

Dredge of carbon nanotubes were dispersed in isopropanol with ultrasonic bath and then disposed on the sample surface. Photolithography and evaporation of metallic mesh were performed before the carbon nanotube deposition to prevent the possible influence of residual photoresist/PMMA[1)] on the work function value of carbon nanotubes [21]. Kelvin probe measurements confirmed that work function values are the same for two samples with SWCNTs and SWCNT bundles measured at different locations on the sample surface. The complete set of measurements was performed on one sample with MWCNTs, two samples with SWCNTs and SWCNT bundles, and one sample with CuI intercalated SWCNTs and SWCNT bundles.

We used three different experimental techniques: topography measurements, Kelvin probe measurements, and measurements of the differential capacitance dC/dz, where z is the tip-to-surface distance.

In our measurements, we used a commercially available scanning probe microscope and cantilever with a diamond coated tip[2)]. Kelvin probe measurements [22] were performed in the dual scan mode. In the first scan, topography information was obtained, and on the second scan, the potential in the Kelvin probe mode was measured. Kelvin probe measurement was performed as follows. An ac voltage at the resonance frequency of the cantilever (f_0) and a dc voltage were applied to the conductive cantilever and mechanical oscillations of the cantilever were detected with a photodiode. A feedback signal was adjusted by the dc voltage to maintain the amplitude of the cantilever oscillations equal to zero. The applied dc voltage was recorded during the second scan.

In the Kelvin probe experiment, the difference in the potential between the tip and the sample was measured, and therefore an additional calibration of the experimental setup was necessary; Pd contacts were used as a material with the known work function. Measurements of the work function of carbon nanotube samples were performed in air conditions. Before measurements, the samples were placed on a hot plate ($T = 110$ °C) for 3 h to remove water from the surface of carbon nanotubes. Values of the measured work function with the Kelvin probe method on carbon nanotubes were stable and reproducible for the next 6 h.

Local differential capacitance measurements were also performed in a dual scan mode [23]. As in Kelvin probe measurements, the first scan gathered topography information and the second scan measured the capacitance itself. During the second scan, the ac signal $f = f_0/2$ was applied to the conductive cantilever and a signal at the frequency f_0 was detected with a photodiode and recorded. This signal is proportional to the differential capacitance dC/dz and is independent of the difference of the dc potential between the tip and the sample.

It was shown previously that noncontact ac and dc electrostatic force measurements allow determining the conductive electron density and the potential distribution in carbon nanotubes, identifying defects or incident changes of the SWCNT chirality, or finding a position of the band gap [24]. Figures 1*b* and 1*c* clearly demonstrate a possibility to use Kelvin probe measurements to gather similar information. Noncontact ac and dc electrostatic force measurements, as well as Kelvin probe measurements, are actually based on the fact that the force of the tip-to-surface interaction is proportional to $(dC/dz)(V_{tip} - V_{surf})$. This value can be extracted from the amplitude of mechanical oscillations of the cantilever while actuation of oscillations and their detection are done at f_0 (V_{tip} and V_{surf} are potentials of the tip of the microscope and of the surface under investigation). Using LCM as a counterpart measurement to extract deviations of the dC/dz value, it is possible to make the surface potential map-

[1)] Polymethil methacrylate.

[2)] We used commercially available scanning probe microscope SP-47 and DCP11 cantilevers by NT-MDT.

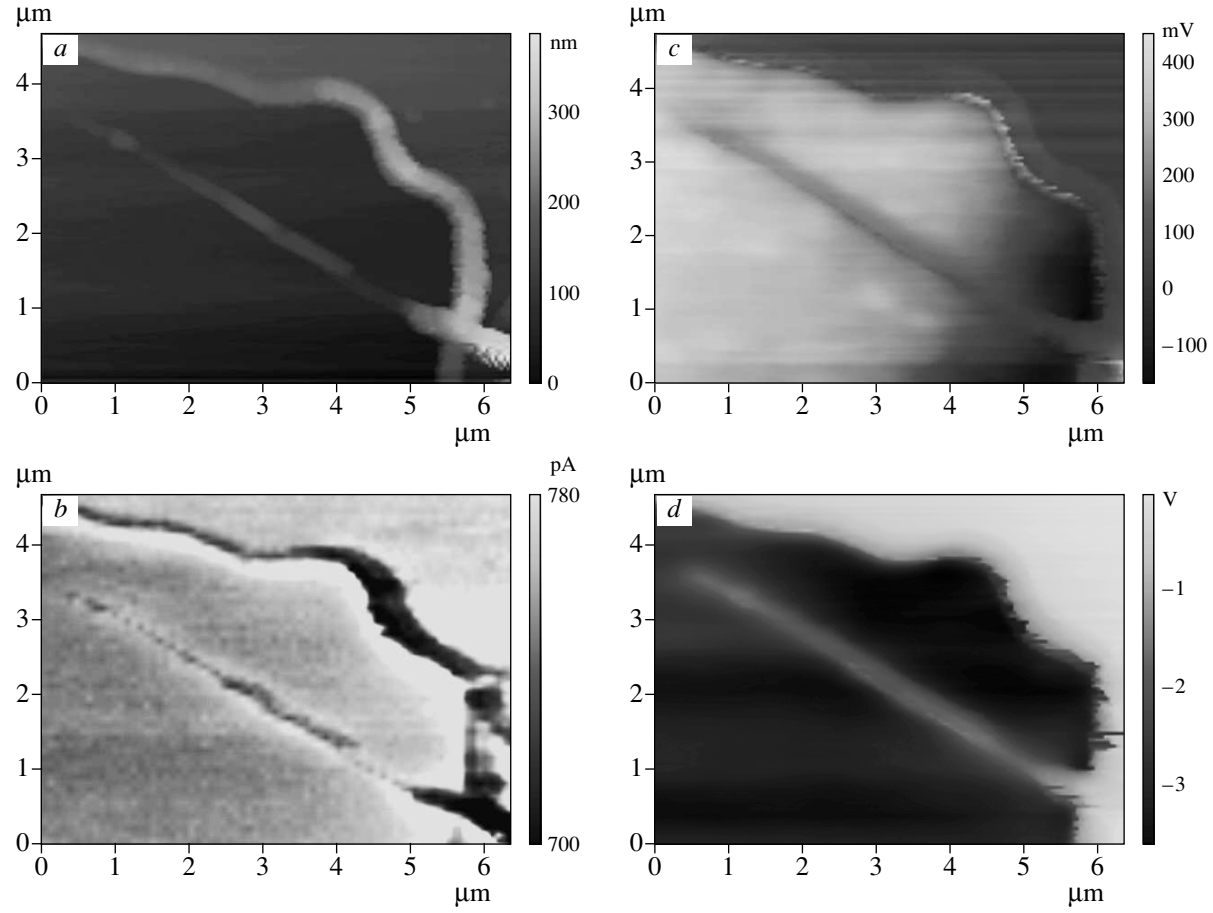

Fig. 1. Topography of an MWCNT sample (a), an LCM scan at $V_{BG} = 0$ V (b), and images made with the Kelvin probe technique at $V_{BG} = 0$ V (c) and $V_{BG} = -5$ V (d). The value of the work function of this carbon nanotube can be extracted from Fig. 1c and is equal to 4.95 eV

ping procedure more reliable. Previously, the value of dC/dz was assumed to be constant [24].

The presence of the metallic mesh and back gate creates an additional possibility of investigating the band structure of carbon nanotubes with the Kelvin probe and LCM techniques. To obtain better resolution, the setup was tuned to minimize the tip-to-surface distance during the second scan, which in some cases produced an interference signal in the Kelvin probe or LCM images originating from the topography of the sample (height steps). The precision of the extracted value of the work function is 0.01 eV.

3. EXPERIMENTAL RESULTS AND DISCUSSION

First, a set of measurements of the work function was carried out on an MWCNT sample. Topography images were first recorded using the nonconducting cantilever to find positions of nanotubes; then the cantilever was changed to the conductive one to perform Kelvin probe and LCM experiments. Scans were acquired at different backgate voltages (V_{BG}) in the range from -10 V to 10 V in order to reveal the whole net of carbon nanotubes. To measure the unbiased value of the work function, the applied backgate voltage was adjusted to minimize the influence of the SiO_2 substrate on the potential of the tube.

The topography image of an MWCNT is presented in Fig 1a; the measured diameter of the tube is 12 nm. Figure 1b presents LCM of the nanotube at $V_{BG} = 0$ V. Brighter regions correspond to higher differential conductivity. It can be clearly seen that the MWCNT has a good conductivity along the whole tube. The same result was obtained in the whole range of backgate voltages from -10 V $\le V_{BG} \le 10$ V. This indicates that at least one metallic shell is present in the MWCNT under investigation. Figures 1c and 1d show experimental Kelvin probe scans at $V_{BG} = 0$ V and $V_{BG} = -5$ V

respectively. Kelvin probe microscopy measurements enabled us to extract the value of the MWCNT work function, $\Phi = 4.95$ eV.

The topography image of a pristine SWCNT sample indicate the presence of both individual SWCNTs with typical diameters 2 nm and SWCNT bundles with diameters 10 nm (Fig. 2*a*). A Kelvin probe measurement at $V_{BG} = 0$ V (Fig. 2*b*) gives the values of the work function in the range 4.95 eV $\leq \Phi \leq$ 4.98 eV for individual SWCNTs and 5.00 eV $\leq \Phi \leq$ 5.05 eV for SWCNT bundles. Figure 2*c* demonstrates a Kelvin probe measurement at $V_{BG} = -5$ V. It is clearly seen that a part of the SWCNT disappears from the Kelvin probe microscopy image. This peculiarity obviously originates in a change of the SWCNT chirality, which essentially decreases its conductivity at low backgate voltages. This peculiarity is also presented at an LCM scan (Fig. 2*d*) done at $V_{BG} = -10$ V.

Figures 3*a* and 3*b* represent the topography image and Kelvin probe measurements at $V_{BG} = 0$ V for a CuI-intercalated SWCNT. The absolute contrast in the Kelvin probe microscopy image, in concert with sample topography, allowed suggesting the presence of three types of SWCNTs characterized by the work function values $\Phi \approx 5$ eV, which is characteristic of pristine SWCNT bundles (the dark-line low left corner in Fig. 3*b* starts from (0 μm, 0 μm) to (1.8 μm, 1.8 μm)); $\Phi \approx$ 4.97–4.98 eV, characteristic of individual SWCNTs (extension from (1.8 μm, 1.8 μm) to (2.3 μm, 2.3 μm)) of the dark-line low left corner in Fig. 3*b* with the transformation from the SWCNT bundle to individual SWCNTs clearly identifiable in the topography mapping picture in Fig. 3*a*; and $\Phi \approx$ 4.86–4.96 eV corresponding to CuI-intercalated SWCNTs (bright curves and spots in Fig. 3*b*). Figure 3*c* presents an LCM scan at $V_{GB} = 0$ V. The conductivity of the whole net of nanotubes is clearly visible and intercalation of CuI does not result in an essential decrease in the conductivity in doped SWCNTs.

The obtained experimental values of the work function of SWCNTs and MWCNTs (4.95–4.98 eV) are similar to and slightly lower than the values of the work function of SWCNT bundles (5.00–5.05 eV). This is in qualitative agreement with theoretical predictions in Ref. [25].

The increase in the work function in tube bundles can be understood if the intertube Van der Waals interactions are taken into account [26]. Our experimental data do not demonstrate a significant variation of the work function values measured on pristine nanotubes, which is in contradiction to other experimental data such as field-emission spectra [27, 28]. But our data are quite similar to secondary-electron photoemission electron microscopy results that demonstrated that nearly 90 % of the work functions of SWCNTs and SWCNT bundles are distributed within an energy range of 0.2 eV [29]. Although the work function can be estimated from the field emission spectra based on the Fowler–Nordheim model, the results are not reliable due to the uncertainty in the local geometry of nanotubes [30]. Intuitively, the deviation of the work function values on the tip of a carbon nanotube looks rather reasonable and many experimental papers insist on electron emission from the tube tips [27]. However, we did not observe significant deviations of the work function on the tips for all kinds of pristine carbon nanotubes in our experiments, which is in good agreement with the secondary-electron photoemission electron microscopy data mentioned above [29].

In Ref. [31], measurements of the work function were performed on MWCNTs. The obtained work function values distributed within an energy range of 0.8 eV are split into two groups, Φ = 4.6–4.8 eV associated with metallic outer-shell MWCNTs and Φ = 5.6 eV semiconducting outer-shell MWCNTs. No significant difference in the values of the work function between metallic and semiconducting SWCNTs was observed in our experiment (see Fig. 2*b*). The measured work function value 4.95 eV of an MWCNT with metallic behavior (see Fig. 1*c*) is quite close to the previously measured values [31].

An application of Kelvin probe microscopy combined with LCM measurements for investigation of CuI-intercalated SWCNTs demonstrates an essential variation of the work function value along the CuI-intercalated SWCNTs (see Fig. 3*b*). This result can be explained by peculiarities of the structure of the one-dimensional CuI nanocrystal inside an SWCNT [18]. As mentioned above, CuI is an acceptor-type dopant [17] and the amount of rearranged charge might depend on the CuI nanocrystal structure, which is not uniquely defined in the SWCNT channel. As a result, the value of the measured work function must vary as well (see Fig. 3*b*). We note that the length of a CuI-intercalated SWCNT with a constant work function (and probably with a single crystal of CuI inside) may exceed one micron and is long enough for possible preparation of a quantum dot with electron-beam lithography. Figure 3*c* shows that reorganization of CuI crystal inside an SWCNT does not essentially change the conductivity of the SWCNT intercalated by CuI at room temperature. To reveal this influence, additional experiments in cryogenic conditions must be performed.

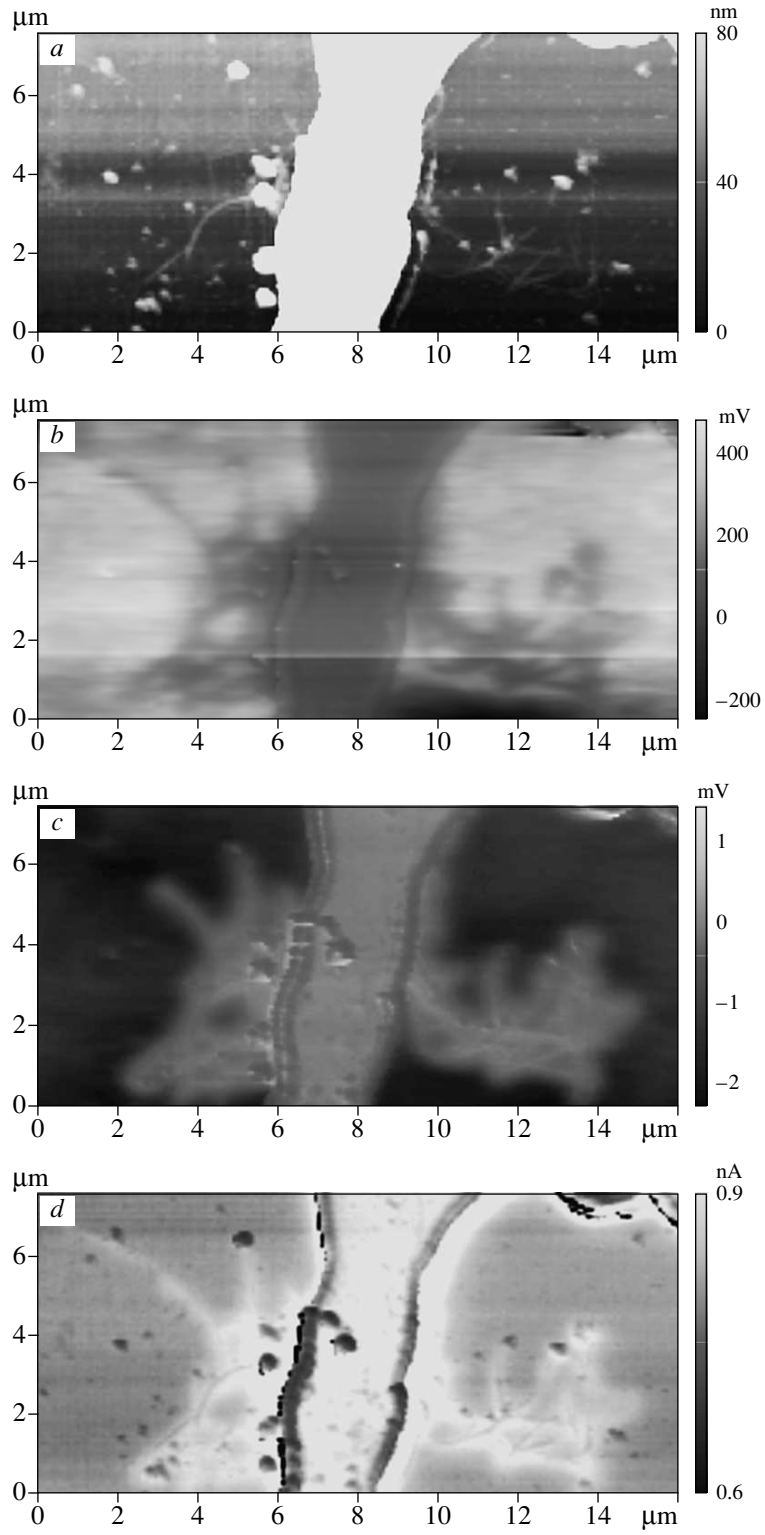

Fig. 2. Topography image of an SWCNT sample (a) and Kelvin probe measurements at $V_{BG} = 0$ V (b) and $V_{BG} = -5$ V (c). Values of the work function in range from 4.95 to 4.98 eV are measured for the SWCNT and values of the work function from 5.00 to 5.05 eV are established for the SWCNT bundle. It is clearly visible that a part of the SWCNT has different chirality and essentially decreases its conductivity at low back gate voltages, so this part of tube disappears from the Kelvin probe scan. A similar feature is presented in the LCM scan d done at $V_{BG} = -10$ V

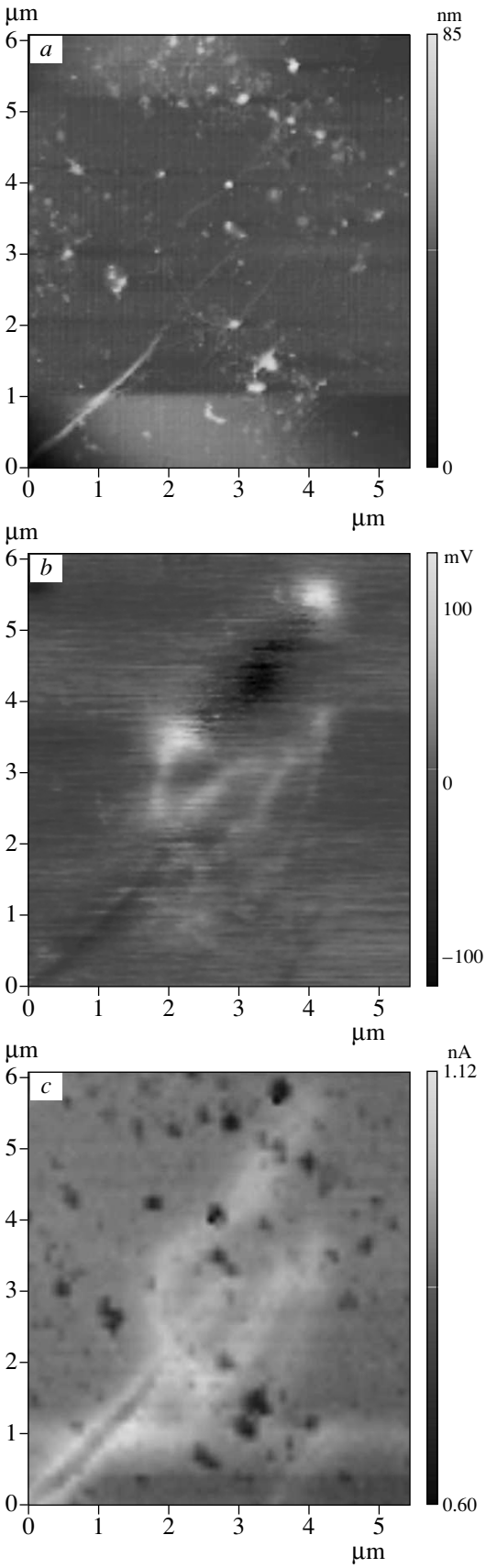

Fig. 3. Topography image of a CuI-intercalated SWCNT sample (a), the Kelvin probe measurement (b), and the LCM scan done at $V_{BG} = 0$ V (c). Two bright spots ((2.3 μm, 3.5 μm) and (4.2 μm, 5.5 μm)) and bright curves are clearly visible on the Kelvin probe scan and reveal positions of CuI impurities inside the SWCNT. A dark line in Fig. 3b is associated with the pristine SWCNT bundle (the line from (0 μm, 0 μm) to (1.8 μm, 1.8 μm)) and with the individual SWCNT (the line from (1.8 μm, 1.8 μm) to (2.3 μm, 2.3 μm)). Obtained values of the work function are $\Phi \approx 5.00$ eV for the SWCNT bundle, $\Phi \approx 4.97$–4.98 eV for the SWCNT, and values of Φ for the CuI-intercalated SWCNT lay in the range from 4.86 to 4.96 eV

4. CONCLUSION

We have performed a set of measurements of carbon nanotube samples using LCM and Kelvin probe techniques. We demonstrate that both the LCM and Kelvin probe noncontact methods can be used to distinguish semiconducting and metallic nanotubes. We confirm the values of the work function of carbon nanotubes and carbon nanotube bundles measured previously with different techniques ($\Phi \approx 4.97$–4.98 eV for SWCNT). For the first time, measurements of the work function were performed for SWCNTs intercalated by CuI. Kelvin probe scans revealed positions of CuI dopants in the SWCNT channel and allowed determining the local value of the work function equal to 4.86–4.96 eV. LCM demonstrated that there is no significant decrease in the conductivity in CuI-doped SWCNTs. The influence of chemical doping on the conductivity of carbon nanotubes at low temperatures is still an open question and requires an additional investigation.

This work is supported by the Russian Foundation for Basic Research (grants Nos. 09-02-00217, 07-02-00098), programs of the Russian Academy of Sciences, and the Program for Support of Leading Scientific Schools.

REFERENCES

1. S. Iijima, Nature **354**, 56 (1991).

2. Ph. Avouris, Z. Chen, and V. Perebeinos, Nature Nanotechnology **2**, 605 (2007).

3. R. Saito, G. Dresselhaus, and M. S. Dresselhaus, *Physical Properties of Carbon Nanotubes*, Imperial College Press, London (1999).

4. L. M. Ang, T. S. A. Hor, G. Q. Xu et al., Carbon **38**, 363 (2000).

5. G.-H. Jeong, A. A. Farajian, R. Hatakeyama et al., Phys. Rev. B **68**, 075410 (2003).

6. X. Fan, E. C. Dickey, P. C. Eklund et al., Phys. Rev. Lett. **84**, 4621 (2000).

7. M. Baenitz and K. Lueders, *Superconductivity in Fullerene Compounds*, Springer Berlin, Heidelberg (2007).

8. B. R. Sankapal, K. Setyowati, and J. Chen, Appl. Phys. Lett. **91**, 173103 (2007).

9. G. Zhao, Qi Zhang, H. Zhang et al., Appl. Phys. Lett. **89**, 263113 (2006).

10. X. Cui, M. Freitag, R. Martel et al., Nano Lett. **3**, 783 (2003).

11. Yu. Miyato, K. Kobayashi, K. Matsushige et al., Jpn. J. Appl. Phys. **44**, 1633 (2005).

12. T. Umesaka, H. Ohnaka, Yu. Ohno et al., Jpn. J. Appl. Phys. **46**, 2496 (2007).

13. G. Riu, A. Verdaguer, F. A. Chaves et al., Microelectron. Eng. **85**, 1413 (2008).

14. D. N. Borisenko, N. N. Kolesnikov, M. P. Kulakov et al., Int. J. Nanoscience **1**, 235 (2002).

15. A. V. Krestinin, M. B. Kislov, and A. G. Ryabenko, in *NATO Science Series*, II. *Mathematics, Physics, and Chemistry*, Vol. 169, ed. by S. Gucery, Y. G. Gogotsi, and V. Kuznetsov, Dordrecht (2004), p. 107.

16. A. V. Krestinin, N. A. Kiselev, A. V. Raevskii et al., Eurasian Chem. Tech. J. **5**, 7 (2003).

17. M. V. Chernysheva, A. A. Eliseev, A. V. Lukashin et al., Physica E **37**, 62 (2007).

18. N. A. Kiselev, R. M. Zakalyukin, O. M. Zhigalina et al., J. Microscopy **232**, 335 (2008).

19. P. Corio, A. P. Santos, P. S. Santos et al., Chem. Phys. Lett. **383**, 475 (2004).

20. M. V. Chernysheva, E. A. Kiseleva, N. I. Verbitskii et al., Physica E **40**, 2283 (2008).

21. H. Hosoi, M. Nakamura, Y. Yamada et al., J. Phys.: Conference Series **100**, 052085 (2008).

22. M. Nonnenmacher, M. P. O'Boyle, and H. K. Wickramasinghe, Appl. Phys. Lett. **58**, 2921 (1991).

23. P. Girard, Nanotechnology **12**, 485 (2001).

24. A. Bachtold, M. S. Fuhrer, S. Plyasunov et al., Phys. Rev. Lett. **84**, 6082 (2000).

25. J. Zhao, J. Han, and J. Ping Lu, Phys. Rev. B **65**, 193401 (2002).

26. P. Delaney, H. J. Choi, J. Ihm et al., Phys. Rev. B **60**, 7899 (1999).

27. W. Zhu, C. Bower, O. Zhou et al., Appl. Phys. Lett. **75**, 873 (1999).

28. A. Wadhawan, R. E. Stallcup II, and J. M. Perez, Appl. Phys. Lett. **78**, 108 (2001).

29. S. Suzuki, Y. Watanabe, Y. Homma et al., Appl. Phys. Lett. **85**, 127 (2004).

30. P. G. Collins and A. Zettl, Phys. Rev. B **55**, 9391 (1997).

31. R. Gao, Zh. Pan, and Zh. L. Wang, Appl. Phys. Lett. **78**, 1757 (2001).